

# Maximizing the electric field strength in the foci of high numerical aperture optics

Markus Sondermann,<sup>1,2,\*</sup> Norbert Lindlein,<sup>1</sup> and Gerd Leuchs<sup>1,2</sup>

<sup>1</sup>*Institute of Optics, Information and Photonics, University of Erlangen-Nuremberg, 91058 Erlangen, Germany*

<sup>2</sup>*Max Planck Institute for the Science of Light, 91058 Erlangen, Germany*

Several applications require spatial distributions of the incident electric field that maximize the electric field at a focal point for a given input power. The field distributions are derived for various optical systems in a direct way based on fundamental physical properties. The results may prove useful for a wide range of applications, e.g., microscopy, scattering experiments or excitation of single atoms. For commonly used distributions - fundamental Gaussian modes and doughnut modes - we give the upper bounds of the achievable field amplitudes.

## I. INTRODUCTION

Recently, there has been increased interest in the interaction of single matter systems like atoms, molecules or ions with weak light beams or single photons in free space. The topical spread covers scattering by single two-level systems [1–5] (including electromagnetically induced transparency[6]) as well as the absorption of single photons by single atoms [7–10]. Also other applications relying on high numerical aperture (NA) optics have raised increasing attention, involving parabolic mirrors [11, 12] as well as lenses [13, 14].

It is common to all these applications that they require the smallest possible focal volume or – in other words – that the power incident onto the focusing optics is transformed in such a way that the electric energy density in the focus is maximized. Thus, one wants to maximize the amplitude of the electric field in the focus. Although it is well known since quite some time that the optimum performance is achieved by electric dipole radiation [15–18] and also some newer publications hint in this direction [13, 19], this recipe is followed only in few papers in a consequent manner [4, 7, 8]. There are also publications in which some sort of 'optimization procedure' is followed: In Ref. [5] the beam width of a circularly polarized fundamental Gaussian is varied in order to maximize the strength of the circularly polarized field component in the focus of an aspheric lens. The authors of Ref. [12] follow a similar procedure in varying the beam waist of a radially polarized doughnut beam during minimization of the focal volume in the case of a parabolic mirror. In both cases, the optimization procedure is equivalent to maximizing the overlap of the incident radiation with dipole radiation. In the former case [5] the Gaussian fundamental mode is matched towards the distribution that creates the field of a circular dipole after refraction by the focusing lens. In the latter case [12] the doughnut mode is adapted such that it best overlaps with the field of a linear dipole that has its axis parallel to the optical axis of the parabolic mirror. Finally, in a recent paper the field distribution that maximizes the focal field component parallel to the optical axis of a high NA lens is directly calculated by a variational method [14] (this concept has been extended to arbitrary orientation of the field vector in Ref. [20]). However, with the exemption of Refs. [12, 13, 21] no direct and

explicit relation between the found optimal radiation modes at the input and a dipole radiation pattern is given in these publications.

Based on earlier results obtained by others [15, 17] we follow a different approach in what follows here. Knowing that it is only electric dipole radiation that contributes to the focal electric field (see, e.g., Refs. [15, 19]), we calculate the distribution of the field incident onto the focusing device that gives the desired dipole radiation pattern after reflection/refraction by the focusing optics, as it was done for a parabolic mirror and linear dipole radiation in Ref. [7]. This approach is on the one hand the most direct one. On the other hand, it is conceptually simple in comparison to other methods. Besides temporal/spectral issues not treated here, this ansatz is the same as the time reversal argument given in Refs. [7, 8, 18] (see also, e.g., Ref. [22] for time reversal focusing of microwaves and Ref. [23] for acoustic waves). [35]

Some of the results obtained here can in parts also be found in other publications [16, 17, 25, 26]. However, a comprehensive study that covers all practically relevant cases is still lacking. Therefore, this paper is intended to deliver a recipe for maximizing the electric field in focusing applications, in particular the excitation of single atoms as envisaged in Refs. [3–5, 8, 10]. In the next section, we will emphasize the importance of a large solid angle of illumination. In Secs. III and IV the optimal intensity and polarization distributions will be derived for the cases of illumination by means of a parabolic mirror, a lens fulfilling the sine condition and an ideal thin lens. Since the experimental realization of these distributions may turn out to be rather involved, the overlap of 'standard' radiation modes with the ideal ones is treated in Sec. V.

Unlike in many other publications where the field in the focal region is treated, the discussion will be restricted to the electric field in the very focal point itself. For the main applications in mind here – scattering by single atoms or absorption of single photons – this constitutes a well justified restriction, since it is only the field at the location of the atom that matters (see also Ref. [4, 5, 19]). Furthermore, this restriction leads to a simple analytical result for the field in the focal point.

## II. INFLUENCE OF THE SOLID ANGLE

Before starting with the calculations, we make some notes on the terminology used in this paper. For the quantum-optical applications mentioned above, the field parallel to an atomic

\*Electronic address: markus.sondermann@physik.uni-erlangen.de

dipole has to be maximized. In these cases, the 'dipole axis' is given by the quantization axis of the scenario at hand. In a classical sense, the term 'dipole axis' designates the direction from which the polar angle  $\vartheta$  is measured that parametrizes the angular dipole radiation patterns (see also Fig. 1). However, one may also think of applications in which no particular emitter or source is present at the focus but one wants to maximize the electric field vector that points into a certain direction (see also Ref. [20]). This field vector can be thought of as being parallel to some imagined dipole moment. Thus, we will adopt the terminology of Ref. [4] and often speak of 'virtual dipoles', i.e., dipoles that *would* produce a certain kind of radiation pattern but are not present in reality.

The term 'solid angle' usually designates the integral over the covered polar angle and the covered azimuthal angle. Here, we will use the term 'weighted solid angle'. It designates the covered solid angle weighted by a certain dipole emission pattern:  $\Omega = \int D(\vartheta) \sin \vartheta d\vartheta d\varphi$ , with  $D_\pi(\vartheta) = \sin^2 \vartheta$  for a linear dipole or  $D_{\sigma_\pm}(\vartheta) = (1 + \cos^2 \vartheta)/2$  for a circular dipole [27], respectively. Thus, the maximum achievable, weighted solid angle is  $\Omega_{\max} = 8\pi/3$  instead of  $4\pi$  in the usual sense. For an incomplete solid angle parametrized by the limits  $\vartheta_{1,2}, \varphi_{1,2}$  one has

$$\Omega_\pi = \left[ \frac{\cos^3 \vartheta}{3} - \cos \vartheta \right]_{\vartheta_1}^{\vartheta_2} \cdot (\varphi_2 - \varphi_1) \quad (1)$$

for a linear dipole and

$$\Omega_{\sigma_\pm} = \frac{1}{2} \left[ -\frac{\cos^3 \vartheta}{3} - \cos \vartheta \right]_{\vartheta_1}^{\vartheta_2} \cdot (\varphi_2 - \varphi_1) \quad (2)$$

for a circular dipole.

We now derive an analytic expression that highlights the influence of the covered weighted solid angle. The electromagnetic field can be decomposed into its different multipole components. This has been exploited in Ref. [25] to calculate the field in the focal region for a given input field. However, since we are only interested in the field at the focus, which we take to coincide with the origin of our coordinate system, we only need to take care of the dipole components. Furthermore, it has already been pointed out in Ref. [16] that each kind of dipole radiation creates predominantly its respective state of polarization at the focus/origin. Therefore, it is obvious that one only needs to create the radiation pattern of a single kind of dipole for most practical cases.

In order to calculate the (time independent) field in the focus, we use the Debye-integral in the form given in Ref. [28]:

$$\mathbf{E}(0) = -i \frac{f}{\lambda} \int \mathbf{E}_f(\vartheta, \varphi) \sin \vartheta d\vartheta d\varphi \quad , \quad (3)$$

where  $\mathbf{E}_f(\vartheta, \varphi)$  is the field on the focal sphere for a focal length  $f$ ,  $\varphi$  is the azimuthal angle and  $\lambda$  the wavelength of the light to be focused. Furthermore, a term  $\exp(i\mathbf{k} \cdot \mathbf{r})$  has already been dropped since we treat only the case  $\mathbf{r} = 0$ .

If only a single kind of dipole radiation is incident onto the focus, the field on the focal sphere can be written as  $\mathbf{E}_f = \psi_d \mathbf{p}_d$ , where  $\psi_d$  is a proportionality factor and  $\mathbf{p}_d$  is

the polarization vector of dipole radiation in the far field with  $d = \pi, \sigma_\pm$  for a linear or circular dipole, respectively. The polarization vectors in spherical coordinates are given by [29]

$$\mathbf{p}_\pi = -\sin \vartheta \mathbf{e}_\vartheta \quad (4)$$

and

$$\mathbf{p}_{\sigma_\pm} = \frac{1}{\sqrt{2}} (\cos \vartheta [\cos \varphi \pm i \sin \varphi] \mathbf{e}_\vartheta + [\pm i \cos \varphi - \sin \varphi] \mathbf{e}_\varphi) \quad (5)$$

with  $\mathbf{e}_{\vartheta, \varphi}$  being the polar and azimuthal unit vectors. Inserting the corresponding polarization vector  $\mathbf{p}_d$  and integrating over the full solid angle for a linear dipole as well as for circular dipoles, the focal field strength is given by

$$E_d^{\max}(0) = -i \frac{f}{\lambda} \psi_d \cdot \frac{8\pi}{3} \quad (6)$$

with the field vector parallel to the (virtual) dipole moment in the focus.

The total power radiated through the surface of the focal sphere can be written as

$$P = \frac{1}{2} \epsilon_0 c f^2 \int_0^{2\pi} \int_0^\pi \psi_d^2 |\mathbf{p}_d|^2 \sin \vartheta d\vartheta d\varphi \quad . \quad (7)$$

The above expression is solved for  $\psi_d$ :

$$\psi_d = \frac{\sqrt{2P}}{f \sqrt{\epsilon_0 c}} \cdot \sqrt{\frac{3}{8\pi}} \quad . \quad (8)$$

This results in the maximum possible field amplitude

$$E_d^{\max}(0) = -i \frac{\sqrt{2P}}{\lambda \sqrt{\epsilon_0 c}} \cdot \sqrt{\frac{8\pi}{3}} \quad . \quad (9)$$

This field delivers the maximum possible electric energy density given earlier by Bassett [15].

We now generalize the treatment to incident fields that do not constitute a perfect dipole wave. In this case only a fraction of the field given by Eq. 9 is expected to be created at the focus. Expanding the incident field on the focal sphere in multipoles and projecting onto the dipole field of interest gives

$$E_d^{\max}(0) = -i \frac{\sqrt{2P}}{\lambda \sqrt{\epsilon_0 c}} \cdot \sqrt{\frac{8\pi}{3}} \cdot \gamma \quad (10)$$

with

$$\gamma = \frac{\int_0^{2\pi} \int_0^\pi \mathbf{p}_d \cdot \mathbf{E}_f \sin \vartheta d\vartheta d\varphi}{\sqrt{\int_0^{2\pi} \int_0^\pi |\mathbf{p}_d|^2 \sin \vartheta d\vartheta d\varphi} \cdot \sqrt{\int_0^{2\pi} \int_0^\pi |\mathbf{E}_f|^2 \sin \vartheta d\vartheta d\varphi}} \quad . \quad (11)$$

All integrals involving  $\mathbf{E}_f$  in the definition of  $\gamma$  need only to be taken in the limits  $\vartheta_{1,2}, \varphi_{1,2}$ , i.e., on the part of the solid

angle for which  $\mathbf{E}_f \neq 0$ . Expanding Eq. 11 with  $\sqrt{\Omega_d}$  one has

$$\gamma = \frac{\sqrt{\Omega_d}}{\sqrt{8\pi/3}} \cdot \eta_d \quad (12)$$

with

$$\eta_d = \frac{\int_{\varphi_1}^{\varphi_2} \int_{\vartheta_1}^{\vartheta_2} \mathbf{p}_d \cdot \mathbf{E}_f \sin \vartheta \, d\vartheta d\varphi}{\sqrt{\Omega_d} \cdot \sqrt{\int_{\varphi_1}^{\varphi_2} \int_{\vartheta_1}^{\vartheta_2} |\mathbf{E}_f|^2 \sin \vartheta \, d\vartheta d\varphi}} \quad (13)$$

being the normalized overlap of the incident electric field with the desired dipole field distribution computed solely on the parts of the focal sphere covered by the incident light. Insertion of Eq. 12 in Eq. 10 yields finally

$$E_d(0) = -i \frac{\sqrt{2P}}{\lambda \sqrt{\epsilon_0 c}} \cdot \sqrt{\Omega_d} \cdot \eta_d \quad (14)$$

This emphasizes that in order to maximize the focal field component parallel to a given virtual dipole one has to (i) put as much of the incident light as possible into the corresponding dipole mode and (ii) maximize the weighted solid angle covered by the incident radiation. It should be pointed out that the resulting field strength does not depend on the dipole type. Furthermore, Eq. 14 constitutes the generalization of Eqs. 8 and 10 of Ref. [14], where the case of a linear dipole oriented along the optical axis of an objective obeying the sine condition is treated. However, the connection to dipole radiation was not established there.

### III. OPTIMUM IRRADIANCE DISTRIBUTIONS

Next, we want to derive the ideal radiation patterns incident onto the focusing device which are transformed into a dipole wave that moves towards the focus. For all devices treated here, we assume that they operate perfectly, i.e., the wave incident onto the focus is assumed to have a uniform phase after reflection/refraction off the focusing device (see also Ref. [12]). For example, a parabolic mirror might exhibit (small) deviations from the perfect parabolic shape. Furthermore, the phase shift upon reflection is different for different angles of incidence. We presuppose that such effects are compensated for by, e.g., appropriate correcting elements. The production of such elements and the measurement of imperfections might turn out to be a challenging but feasible experimental task [30].

The method is simply to start with a dipole wave which virtually emerges from the focus and trace it back through the optical element under consideration. We have chosen to formulate the ideal radiation patterns in terms of irradiances instead of field vectors, since the former quantity is the one usually measured in an experiment. Furthermore, in the derivation of the apodization factors carried out below, energy conservation considerations require the use of irradiances and radiant intensities anyway. The ideal vector fields can be constructed from

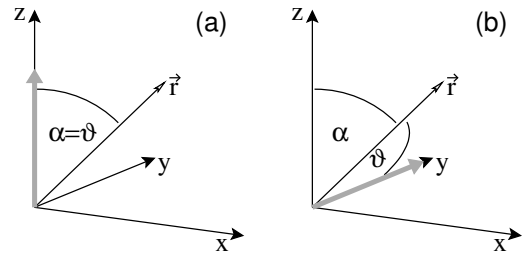


FIG. 1: Relation of the angles  $\alpha$  and  $\vartheta$  to the Cartesian coordinates: (a) dipole/quantization axis (gray arrow) parallel to the optical axis; (b) dipole/quantization axis perpendicular to the optical axis.

the irradiance patterns and the polarization patterns derived in the next section.

The derivation of the intensity patterns is pursued in the same way as it was done in Ref. [7] for a parabolic mirror and a linear dipole oriented parallel to the optical axis of the mirror. We designate by  $\alpha$  the angle that is enclosed by the optical axis of the focusing element and the propagation direction of a single ray which hits the optical element at a distance  $r$  from the optical axis. Here, we chose the optical axis to coincide with the  $z$ -axis (cf. Fig. 1). Energy conservation demands that [7]

$$\Upsilon(\alpha) \sin \alpha \, d\alpha = I(r) r \, dr \quad (15)$$

which delivers

$$I(r) = \Upsilon(\alpha) \cdot A(r, \alpha) \quad (16)$$

with  $A(r, \alpha) = \frac{\sin \alpha(r)}{r} \frac{d\alpha(r)}{dr}$  being an apodization factor.  $\Upsilon(\alpha)$  is the radiant intensity, i.e., the light power emitted into an infinitesimal solid angle.  $I(r)$  is the irradiance of the incident plane wave, i.e., the light power incident onto an infinitesimal surface area.

In what follows, we express the apodization factor as a function of the Cartesian coordinates  $x, y$  in the plane perpendicular to the optical axis:  $A(x, y) = A(r(x, y))$  with  $r = \sqrt{x^2 + y^2}$ . In the case of a parabolic mirror,  $\alpha$  is given through the relation [7]

$$\tan \frac{\alpha}{2} = \frac{r}{2f} \quad (17)$$

which with the help of some algebra leads to

$$A_{PM}(x, y) = \frac{1}{f^2 \left( \frac{x^2}{4f^2} + \frac{y^2}{4f^2} + 1 \right)^2} \quad (18)$$

For an aplanatic lens that fulfills the sine condition, i.e., a lens where the refracted rays of same phase seem to emerge from a spherical surface around the focus, one has

$$\sin \alpha = \frac{r}{f} \quad (19)$$

resulting in

$$A_{AL}(x, y) = \frac{1}{f^2 \sqrt{1 - \frac{x^2}{f^2} - \frac{y^2}{f^2}}} \quad (20)$$

As a third focusing element, we consider an ideal thin lens, i.e., a lens for which the refracted rays seem to emerge from a plane perpendicular to the optical axis. A practical realization of such a thin lens would be an idealized diffractive optical lens (e.g., as used recently for imaging ion fluorescence [31]). One has

$$\tan \alpha = \frac{r}{f}, \quad (21)$$

which delivers

$$A_{TL}(x, y) = \frac{1}{f^2 \left( \frac{x^2}{f^2} + \frac{y^2}{f^2} + 1 \right)^{3/2}}. \quad (22)$$

Next, for every point  $(x, y)$  in the plane perpendicular to the optical axis we determine  $\vartheta$ . The radiant intensity along this direction is given by the angular dipole radiation pattern  $D(\vartheta)$ :

$$\Upsilon(\vartheta) = D_0 \cdot D(\vartheta), \quad (23)$$

where  $D_0$  is a proportionality constant. Finally,  $\Upsilon(\vartheta)$  is also expressed in terms of  $x, y$  and multiplied with the apodization factor  $A(x, y)$  yielding the irradiance  $I(x, y)$ .

If the dipole is oriented parallel to the optical axis,  $\alpha$  coincides with  $\vartheta$  (see Fig. 1a). Hence, the ideal irradiation is rotationally symmetric with respect to the optical axis and the angular dipole emission patterns given above can be written as  $D_{\pi, \sigma_{\pm}}(\vartheta) = D_{\pi, \sigma_{\pm}}(\alpha)$ . Using Eqs. 17, 19 and 21, respectively, and applying several trigonometric relations one obtains the ideal irradiance distributions. They are summarized in Tab. I and plotted in Fig. 2. We have also introduced normalized coordinates  $X = x/f, Y = y/f, R = r/f$ . All remaining dimensional quantities have been lumped into a proportionality constant  $I_0$ .

The formula obtained here for the irradiance in the case of an aplanatic lens fulfilling the sine condition and a linear dipole corresponds exactly to the square of the formula for the electric field amplitude in the entrance pupil of the lens as it was found by means of an optimization method in Ref. [14].

Next, we turn to the case of the virtual dipole being oriented perpendicular to the optical axis of the focusing element. Without loss of generality we choose the virtual dipole axis (the direction  $\vartheta=0$ ) to coincide with the  $y$ -axis (see Fig. 1b). An immediate consequence of the dipole axis being orthogonal to the optical axis is that the ideal intensity distributions have no longer rotational symmetry with respect to the optical axis. Furthermore, the angles  $\alpha$  and  $\vartheta$  do not coincide any more. Thus, the relations given by Eqs. 17, 19 and 21 cannot be used to express the angular emission patterns  $D_{\pi, \sigma_{\pm}}(\vartheta)$  in terms of the transverse coordinates. Instead one has to use in the case of the parabolic mirror the relations

$$\cos \vartheta = \frac{y}{\sqrt{x^2 + y^2 + z^2}}, \quad z = f - \frac{x^2 + y^2}{4f}. \quad (24)$$

This is valid if the focus of the parabolic mirror is located in the origin of the coordinate system. For a lens obeying the

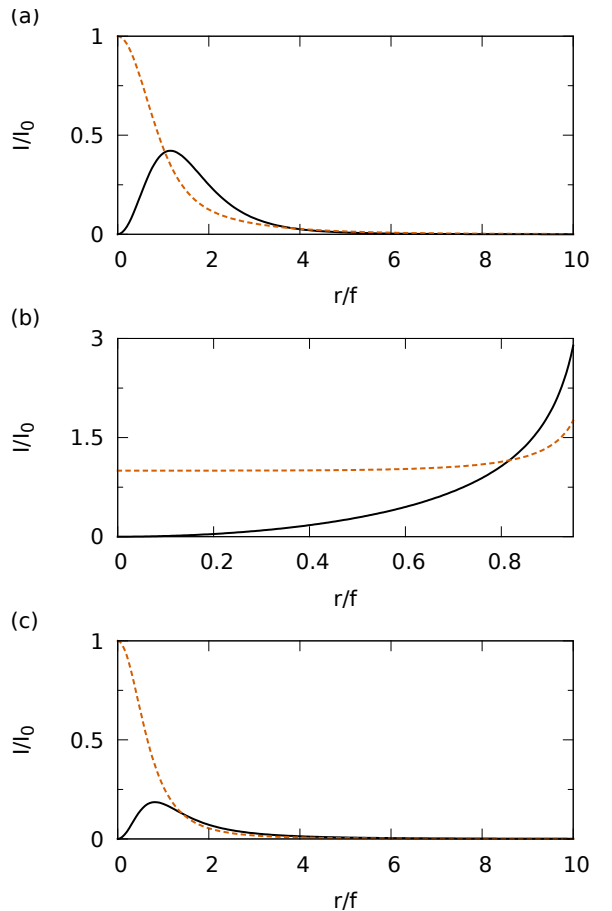


FIG. 2: Ideal irradiance distributions for dipoles oriented parallel to the optical axis of the focusing device: (a) parabolic mirror, (b) aplanatic lens fulfilling the sine condition, (c) ideal thin lens. Solid (dashed) lines denote the irradiance for a linear (circular) dipole radiation pattern.

sine condition the relation between  $\vartheta$  and  $x, y$  reads

$$\cos \vartheta = \frac{y}{f}, \quad (25)$$

and for the ideal thin lens one has

$$\tan \vartheta = \frac{\sqrt{x^2 + f^2}}{y}. \quad (26)$$

Again, the focus is located in the origin of the coordinate system. Using some trigonometric relations and multiplication with the corresponding apodization factors leads to the ideal irradiance distributions given in Tab. II and displayed in Fig. 3.

#### IV. OPTIMUM STATES OF POLARIZATION

We begin the discussion for a virtual dipole parallel to the optical axis. For a linear dipole, the polarization pattern can be obtained immediately from the fact that the polarization

TABLE I: Optimum irradiance distributions  $I(R)$  for the creation of radiation patterns of dipoles oriented parallel to the optical axis of the focusing device.  $R = r/f$  is the radial coordinate transverse to the optical axis given in units of the focal length. The proportionality constant  $I_0$  contains all dimensional quantities.

	parabolic mirror	aplanatic lens	ideal thin lens
linear dipole	$I_0 \cdot \frac{R^2}{(\frac{R^2}{4} + 1)^4}$	$I_0 \cdot \frac{R^2}{\sqrt{1 - R^2}}$	$I_0 \cdot \frac{R^2}{(R^2 + 1)^{\frac{5}{2}}}$
circular dipole	$I_0 \cdot \frac{\frac{R^4}{16} + 1}{(\frac{R^2}{4} + 1)^4}$	$I_0 \cdot \frac{1 - \frac{R^2}{2}}{\sqrt{1 - R^2}}$	$I_0 \cdot \frac{1 + \frac{R^2}{2}}{(R^2 + 1)^{\frac{5}{2}}}$

TABLE II: Optimum irradiance distributions  $I(X, Y)$  for the creation of radiation patterns of dipoles oriented orthogonal to the optical axis of the focusing device.  $X = x/f$  and  $Y = y/f$  are the coordinates transverse to the optical axis given in units of the focal length. The proportionality constant  $I_0$  contains all dimensional quantities.

	parabolic mirror	aplanatic lens	ideal thins lens
linear dipole	$I_0 \cdot \frac{1 - \frac{Y^2}{X^2 + Y^2 + (X^2/4 + Y^2/4 - 1)^2}}{(X^2/4 + Y^2/4 + 1)^2}$	$I_0 \cdot \frac{1 - Y^2}{\sqrt{1 - X^2 - Y^2}}$	$I_0 \cdot \frac{1 + X^2}{(X^2 + Y^2 + 1)^{5/2}}$
circular dipole	$I_0 \cdot \frac{1/2 + \frac{Y^2/2}{X^2 + Y^2 + (X^2/4 + Y^2/4 - 1)^2}}{(X^2/4 + Y^2/4 + 1)^2}$	$I_0 \cdot \frac{1/2 + Y^2/2}{\sqrt{1 - X^2 - Y^2}}$	$I_0 \cdot \frac{Y^2 + \frac{X^2 + 1}{2}}{(X^2 + Y^2 + 1)^{5/2}}$

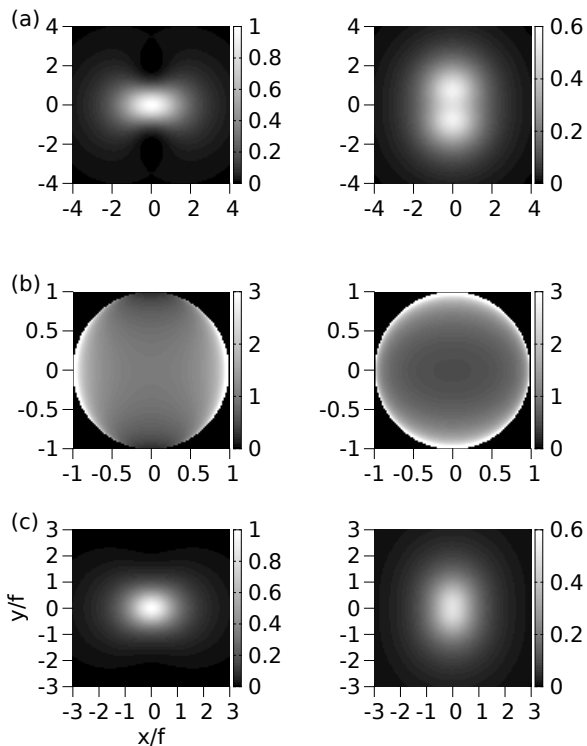


FIG. 3: Ideal irradiance distributions for dipoles oriented orthogonal to the optical axis of the focusing device: (a) parabolic mirror, (b) lens fulfilling the sine condition, (c) ideal thin lens. Left panel: linear dipole; right panel: circular dipole. The gray levels designate the values of  $I/I_0$ .

vector of a linear dipole is oriented along  $\mathbf{e}_\vartheta$  in the far field. This results in the well known radial polarization pattern [7, 13, 18] and, of course, coincides with the result found recently by optimization [14]. The polarization pattern is the same for all of the devices discussed here.

The situation is slightly more complex in the case of a circular dipole. The polarization vector for a certain  $\vartheta$  is given by  $\mathbf{p}_{\sigma_\pm}$  in Eq. 5. Using the relations given in Ref. [32] the normalized Stokes parameter  $S_3/S_0$  describing the degree of circular polarization is readily determined to be

$$\frac{S_{3\sigma_\pm}}{S_{0\sigma_\pm}} = \frac{\pm 2 \cos \vartheta}{1 + \cos^2 \vartheta}, \quad (27)$$

where  $S_0$  corresponds to the total intensity and  $S_3$  to the intensity that would be measured after passing the beam through a circular polarizer. With  $S_3/S_0 = \sin(2\chi)$  giving the so called ellipticity angle [33], the ellipticity as a function of  $\vartheta$  is

$$\chi_{\sigma_\pm} = \frac{\arcsin\left(\frac{\pm 2 \cos \vartheta}{1 + \cos^2 \vartheta}\right)}{2}, \quad (28)$$

where  $\chi_{\sigma_\pm} = \pm\pi/4$  corresponds to circular states of polarization. This shows that the ideal polarization pattern for circular dipoles exhibits a varying ellipticity as a function of the radial distance to the optical axis.

Using Eqs. 17, 19 and 21 to express  $\vartheta$  through  $r$ , one obtains the ideal state of polarization for the different focusing devices. The results are displayed in Fig. 4. Note that in the case of the parabolic mirror there is a sign change of the ellipticity at the radius  $r = 2f$ , which corresponds to a half opening angle of the parabolic mirror of  $90^\circ$ . This result explains the finding of Ref. [12](Fig. 2) that an increase of the

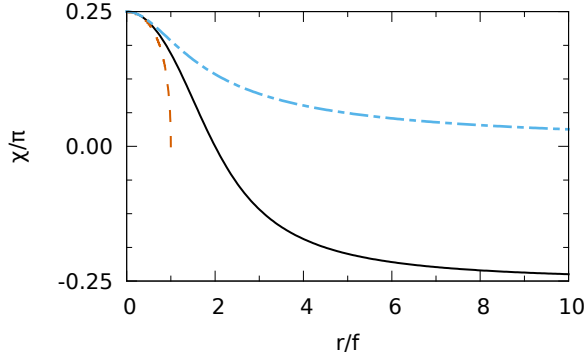


FIG. 4: Ellipticity of the ideal states of polarization for a circular dipole ( $\sigma_+$ , a sign change gives the values for  $\sigma_-$ ) oriented parallel to the optical axis of the focusing device. Solid line: parabolic mirror; dashed line: aplanatic lens; dash-dotted line: ideal thin lens.

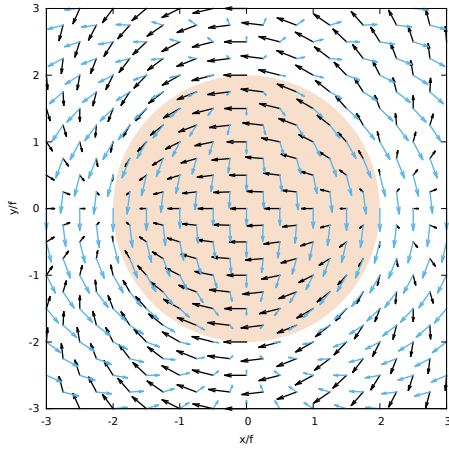


FIG. 5: State of polarization of the ideal radiation pattern for the case of a parabolic mirror and a circular dipole ( $\sigma_+$ ) with the dipole axis oriented parallel to the optical axis of the mirror. The vectors in light blue color denote the linearly polarized components with  $\pi/2$  phase shift. The shaded area denotes the region of NA=1.

half focusing angle beyond  $90^\circ$  does not lead to a substantial decrease of focus size for an incident wave that has a circular state of polarization of same helicity over the whole beam cross section.

The spatial polarization pattern in the entrance plane of the focusing devices is calculated exemplarily for a parabolic mirror. First,  $\mathbf{p}_{\sigma_\pm}$  is transformed into a unit vector  $\hat{\mathbf{p}}_{\sigma_\pm}$  by multiplication with  $\sqrt{2}/\sqrt{1 + \cos^2 \vartheta}$ . Then, the polarization pattern after reflection off the parabolic mirror is obtained as follows: The state of polarization  $\hat{\mathbf{p}}_{\vartheta, \varphi}$  of the virtual dipole, formulated in terms of the spherical unit vectors  $\mathbf{e}_{\vartheta, \varphi}$ , is transformed into the Cartesian coordinate system:  $\hat{\mathbf{p}}_{\vartheta, \varphi} \rightarrow \hat{\mathbf{p}}_{x, y, z}$ . Then, the ray for each emission direction is traced from the virtual dipole towards the surface of the parabolic mirror. The polarization vector of the ray after reflection at the mirror surface is calculated via the following equation:

$$\hat{\mathbf{p}} = 2(\hat{\mathbf{p}}_{x, y, z} \cdot \mathbf{N})\mathbf{N} - \hat{\mathbf{p}}_{x, y, z} \quad , \quad (29)$$

with the surface normal of the mirror given by

$$\mathbf{N} = \frac{1}{\sqrt{\frac{x^2 + y^2}{4f^2} + 1}} \begin{pmatrix} \frac{x}{2f} \\ \frac{y}{2f} \\ 1 \end{pmatrix} \quad . \quad (30)$$

Again, the focus is chosen to be at the origin of the coordinate system. For  $\sigma_\pm$  light, this procedure results in

$$\hat{\mathbf{p}}_{\sigma_\pm}(X, Y) = \frac{1}{\sqrt{2[(X^2 + Y^2)^2 + 16]}} \times \left[ \begin{pmatrix} X^2 - Y^2 - 4 \\ 2XY \end{pmatrix} \pm i \begin{pmatrix} 2XY \\ Y^2 - X^2 - 4 \end{pmatrix} \right] \quad . \quad (31)$$

This pattern is depicted in Fig. 5. Up to the boundary given by  $\sqrt{X^2 + Y^2} = 2$  (or numerical aperture NA=1), the polarization pattern is qualitatively similar for the other focusing devices treated here. However, one has to keep in mind that the relations between  $\vartheta, \varphi$  and the Cartesian coordinates in the entrance plane of the devices are different. Thus, the pattern displayed inside the circle marking NA=1 in Fig. 5 will be distorted or stretched/compressed to some amount, respectively.

If the dipole axis is orthogonal to the optical axis, the procedure is the same except that in this case the direction  $\vartheta = 0$  coincides with the positive  $y$ -axis. This is handled by interchanging the second with the third component of the unit vectors  $\mathbf{e}_{\vartheta, \varphi}$  of the spherical coordinate system. Using Eqs. 4 and 5, one obtains the polarization patterns

$$\hat{\mathbf{p}}_{\pi}(X, Y) = \frac{1}{\sqrt{(X^2 + Y^2 + 4)^2 - 16Y^2}} \begin{pmatrix} 2XY \\ Y^2 - X^2 - 4 \end{pmatrix} \quad (32)$$

for a linear dipole and

$$\hat{\mathbf{p}}_{\sigma_\pm}(X, Y) = \frac{1}{\sqrt{16Y^2 + (4 + X^2 + Y^2)^2}} \times \left[ \begin{pmatrix} X^2 - Y^2 - 4 \\ 2XY \end{pmatrix} \pm i \begin{pmatrix} 4X \\ 4Y \end{pmatrix} \right] \quad (33)$$

for the circular dipoles. The two polarization patterns are illustrated in Fig. 6.

## V. OVERLAP OF PRACTICAL DISTRIBUTIONS WITH THE IDEAL ONES

Some of the radiation patterns derived above – especially in the case of the dipole axis parallel to the optical axis – exhibit obvious similarities with radiation modes which are commonly used in experiments. In the case of a parabolic mirror and the ideal thin lens, the irradiance distributions for a linear virtual dipole look close to the well known doughnut modes. In the case of circular virtual dipoles there is a strong similarity with fundamental Gaussian distributions.

In order to estimate and quantify the strength of the similarities, we will calculate the overlap of these modes with the

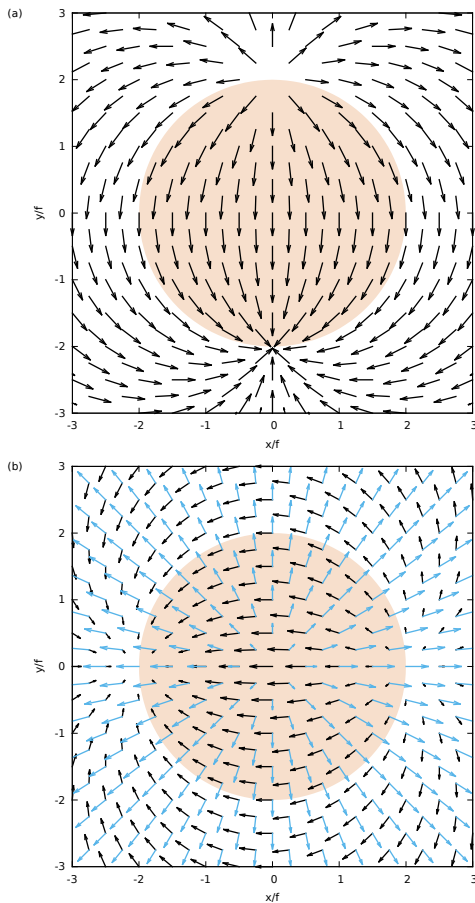


FIG. 6: State of polarization of the ideal radiation patterns for the case of a parabolic mirror and the dipole axis oriented orthogonal to the optical axis of the mirror: (a) linear dipole, (b) circular dipole ( $\sigma_+$ ). In (b) the vectors in light blue color denote the linearly polarized components with  $\pi/2$  phase shift. The shaded area denotes the region of NA=1.

ideal radiation distributions. We begin with recalling that the transformation of the field distribution in the entrance plane of the focusing device to the one on the focal sphere is of course the same for the ideal dipole fields and the incident fields. Therefore, it does not matter whether the overlap  $\eta_d$  in Eq. 14 is calculated on the focal sphere or in the entrance aperture of the focusing optics. Since the field in the entrance aperture is the one that is more easily accessible in experiments, all overlaps are calculated there in what follows.

Figure 7 shows some examples for illustration. In the case of a parabolic mirror with a half opening angle of  $134^\circ$  as it is used in the experiment described in Refs. [7, 8], a radially polarized doughnut mode ( $\sqrt{I(r)} \sim r \cdot e^{-r^2/w^2}$ ,  $w$  is the beam radius) best matches the field distribution for a linear dipole parallel to the optical axis at a beam radius of  $w/f = 2.26$ . There, the overlap is  $\eta_\pi = 0.982$ . The half opening angle of  $134^\circ$  corresponds to  $\Omega_\pi = 0.94 \times 8\pi/3$ . Thus, the field amplitude parallel to the virtual linear dipole would be 0.95 times the one obtained with the ideal radiation pattern and a parabolic mirror of infinite dimensions. This has

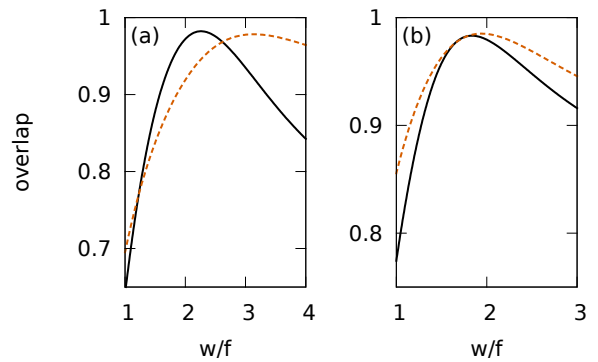


FIG. 7: Normalized overlap of the ideal field distributions with common radiation modes as a function of the modes beam radius  $w$  in units of the focal length  $f$ . The virtual dipoles are oriented parallel to the optical axis. (a) Parabolic mirror with a half opening angle of  $134^\circ$ . (b) Ideal thin lens with a numerical aperture of 0.95. Solid lines: Overlap of the ideal field for linear dipoles with a radially polarized doughnut mode. Dashed lines: Overlap of the ideal field for circular dipoles with a fundamental Gaussian mode that has an ideal state of polarization.

been confirmed in simulations. In the case of a circular dipole parallel to the optical axis, the maximum overlap of  $\eta_{\sigma_\pm} = 0.978$  is achieved for a Gaussian fundamental mode ( $\sqrt{I(r)} \sim e^{-r^2/w^2}$ ) with a beam waist of  $w/f = 3.14$ . With  $\Omega_{\sigma_\pm} = 0.80 \times 8\pi/3$  one achieves a field amplitude parallel to the virtual circular dipole of 0.87 times the maximum possible one.

For an ideal thin lens and dipoles parallel to the optical axis (Fig. 7b) with NA=0.95 the optimum overlap of  $\eta_\pi = 0.983$  is reached at  $w/f = 1.84$  (linear dipole) and the maximum value of  $\eta_{\sigma_\pm} = 0.985$  reached at  $w/f = 1.94$  (circular dipole). With  $\Omega_\pi = 0.27 \times 8\pi/3$  and  $\Omega_{\sigma_\pm} = 0.38 \times 8\pi/3$  one achieves 0.51 and 0.61 times the field amplitudes of the maximum possible ones, respectively.

Please note that for the parabolic mirror as well as for the ideal thin lens the optimum beam waist of the doughnut is such that the maximum of the irradiance distribution is located at a somewhat larger radial position than the maximum of the radiation patterns of a linear dipole that are displayed in Fig. 2(a,c). Furthermore, the values for the circular dipoles given above have to be considered as upper limits in the sense that the ideal state of polarization for a circular dipole is difficult to obtain in practice (see below).

If the weighted solid angle covered by the focusing optics is increased, the maximum achievable overlap of the 'simple' modes with the ideal distributions decreases. However, this is overcompensated for by the increase in weighted solid angle, i.e., the field in the focus parallel to a specific virtual dipole is maximized by maximizing the weighted solid angle. This is illustrated in Fig. 8(a) for a linear dipole parallel to the optical axis and a parabolic mirror (illuminated by a radially polarized doughnut). For each (half) opening angle of the mirror the maximum overlap is obtained from a curve like the one in Fig. 7(a). The resulting field is then obtained from Eq. 14 by

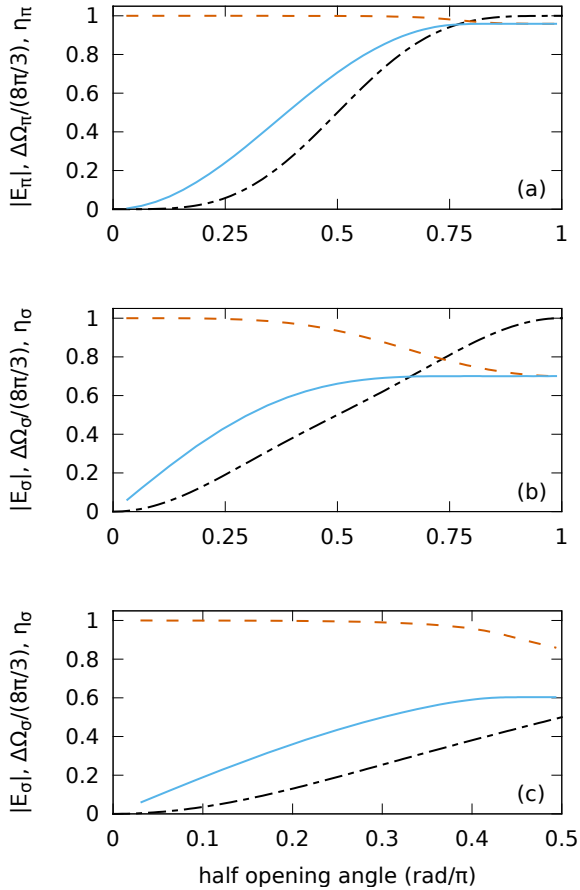


FIG. 8: Weighted solid angle  $\Omega_d/(8\pi/3)$  (dash-dotted line), maximum possible overlap  $\eta_d$  with a linear dipole wave (dashed line) and field amplitude  $|E_d|$  in the focus in units of the maximum possible one (solid line) as a function of the half opening angle for (a) a parabolic mirror illuminated by a radially polarized doughnut mode, (b) a parabolic mirror illuminated by a circularly polarized fundamental Gaussian and (c) an ideal thin lens illuminated by a circularly polarized fundamental Gaussian. For further explanations see text.

inserting the overlap value and the corresponding square root of the covered weighted solid angle into this equation.

From the asymptotic behavior of the plot for the field amplitude in Fig. 8(a) one can extract the maximum field amplitude one could achieve with a doughnut mode of suitable polarization by focusing the mode with a parabolic mirror. Likewise, one obtains the same values for circular dipoles (i.e., overlapping with a Gaussian mode of proper polarization) and/or an ideal thin lens. The values are listed in Tab. III.

So far, we have assumed modes with an ideal state of polarization. As an illustration we now treat the fields obtainable with circularly polarized fundamental Gaussian modes. For a parabolic mirror and a circular dipole parallel to the optical axis the maximum achievable overlap drops significantly at about half opening angles of  $\pi/2$  (cf. Fig. 8b). Likewise, the corresponding field in the focal point saturates at this value. We attribute this behavior to the change of the helicity of the ideal polarization pattern at  $\pi/2$  half opening angle. In other

TABLE III: Maximum electric field amplitudes achievable by use of a radially polarized doughnut mode and a fundamental Gaussian mode with the state of polarization matching a circular dipole. The values are given relative to the ones obtainable with the ideal irradiance distributions of Fig. 2(a,c). The virtual dipoles are oriented parallel to the optical axis.

	doughnut mode	fundamental Gaussian
parabolic mirror	0.958	0.919
ideal thin lens	0.575	0.628

words, the uniformly circular polarized beam is strongly mismatched to the ideal pattern at larger angles. For full solid angle, the field strength approaches 0.7 times the maximum possible one. Hence, the imperfect polarization state drastically limits the attainable field strength and an increase of the mirror size beyond half solid angle does not result in a significant gain of the focal field amplitude.

Figure 8(c) treats the case of an ideal thin lens that is illuminated by a circularly polarized fundamental Gaussian beam. If the NA approaches a value of 1, the maximum achievable field tends to 0.603 times the one for a perfect dipole wave. This value corresponds perfectly to the one found in Ref. [5] for the same setup. Moreover, the corresponding beam radius that gives the best overlap is exactly the same that is found there.

For the case of a lens obeying the sine condition the calculation of the overlap with the simple modes discussed above does not appear to be meaningful on first sight. This is due to the divergence of the ideal irradiance values towards the boundary of the lens aperture. Nevertheless, large overlaps can be achieved if the beam radius tends towards values larger than the aperture size. For example, for an objective with  $\text{NA}=0.95$  the overlap of a radially polarized doughnut mode with the ideal dipole field is 0.927 if the beam radius matches the aperture radius. However, already for this value roughly 40% of the power contained in the doughnut mode is cut off by the aperture boundary. At even larger beam radii the overlap saturates at a value of about 0.989 by the cost of losing practically all photons contained in the doughnut mode at the lens aperture.

Likewise, the overlap of a linearly polarized fundamental Gaussian mode with the ideal field of a linear dipole oriented *orthogonal* to the optical axis increases continuously with beam radius for an aplanatic lens. For  $\text{NA}=0.95$  the overlap is 0.927 if beam radius and aperture radius are equal (14% loss of power by cutting off the tail of the Gaussian mode). The overlap for much larger beam radii is saturating at about 0.972.

## VI. CONCLUDING REMARKS

We have derived the ideal radiation patterns with which one achieves the maximum possible field strengths for several focusing devices. Besides using these radiation patterns, it is of utmost importance to maximize the covered weighted solid



angle, as it is shown by Eq. 14. Thus, the maximum possible electric field strength is achieved by covering the full solid angle. Also, the maximum possible effect in the interaction of light with single atoms will also only be found for full solid angle coverage, since scattering as well as absorption of photons is proportional to the square of the electric field amplitude

at the location of the atom [32]. According with the papers of Van Enk and Kimble [19, 34], we want to stress once more that for optimum interaction of light with single atoms one has to shape the radiation incident onto the atom to resemble an electric dipole wave.

- 
- [1] A. N. Vamivakas, M. Atatüre, J. Dreiser, S. T. Yilmaz, A. Badolato, A. K. Swan, B. B. Goldberg, A. Imamoglu, and M. S. Ünlü, *Nano Letters* **7**, 2892 (2007).
- [2] G. Wrigge, I. Gerhardt, J. Hwang, G. Zumofen, and V. Sandoghdar, *Nature Physics* **4**, 60 (2008).
- [3] M. K. Tey, Z. Chen, S. A. Aljunid, B. Chng, F. Huber, G. Maslennikov, and C. Kurtsiefer, *Nature Physics* **4**, 924 (2008).
- [4] G. Zumofen, N. M. Mojarad, V. Sandoghdar, and M. Agio, *Phys. Rev. Lett.* **101**, 180404 (2008).
- [5] M. K. Tey, G. Maslennikov, T. C. H. Liew, S. A. Aljunid, F. Huber, B. Chng, Z. Chen, V. Scarani, and C. Kurtsiefer, *New Journal of Physics* **11**, 043011 (2009).
- [6] L. Slodička, G. Hétet, S. Gerber, M. Hennrich, and R. Blatt, *Phys. Rev. Lett.* **105**, 153604 (2010).
- [7] N. Lindlein, R. Maiwald, H. Konermann, M. Sondermann, U. Peschel, and G. Leuchs, *Laser Physics* **17**, 927 (2007).
- [8] M. Sondermann, R. Maiwald, H. Konermann, N. Lindlein, U. Peschel, and G. Leuchs, *Appl. Phys. B* **89**, 489 (2007).
- [9] D. Pinotsi and A. Imamoglu, *Phys. Rev. Lett.* **100**, 093603 (2008).
- [10] N. Piro, F. Rohde, C. Schuck, M. Almendros, J. Huwer, J. Ghosh, A. Haase, M. Hennrich, F. Dubin, and J. Eschner, *Nat. Phys.* **7**, 17 (2011).
- [11] J. Stadler, C. Stanciu, C. Stupperich, and A. J. Meixner, *Opt. Lett.* **33**, 681 (2008).
- [12] N. Bokor and N. Davidson, *Opt. Commun.* **281**, 5499 (2008).
- [13] N. Bokor and N. Davidson, *Opt. Lett.* **29**, 1968 (2004).
- [14] H. P. Urbach and S. F. Pereira, *Physical Review Letters* **100**, 123904 (2008).
- [15] I. M. Bassett, *Journal of Modern Optics* **33**, 279 (1986).
- [16] J. J. Stamnes and V. Dhayalan, *Pure Appl. Opt.* **5**, 195 (1996).
- [17] C. J. R. Sheppard and P. Török, *Optik* **104**, 175 (1997).
- [18] S. Quabis, R. Dorn, M. Eberler, O. Glöckl, and G. Leuchs, *Opt. Comm.* **179**, 1 (2000).
- [19] S. J. van Enk, *Phys. Rev. A* **69**, 043813 (2004).
- [20] H. P. Urbach and S. F. Pereira, *Phys. Rev. A* **79**, 013825 (2009).
- [21] W. Chen and Q. Zhan, *Journal of Optics* **12**, 045707 (2010).
- [22] G. Lerossey, J. de Rosny, A. Tourin, A. Derode, G. Montaldo, and M. Fink, *Phys. Rev. Lett.* **92**, 193904 (2004).
- [23] J. de Rosny and M. Fink, *Phys. Rev. Lett.* **89**, 124301 (2002).
- [24] We note that recently the approach we follow here has been applied for the case of an aplanatic lens [21].
- [25] C. J. R. Sheppard and P. Török, *J. Mod. Opt.* **44**, 803 (1997).
- [26] V. Dhayalan and J. J. Stamnes, *Pure Appl. Opt.* **6**, 347 (1997).
- [27] J. D. Jackson, *Classical Electrodynamics* (Wiley, New York, 1999), 3rd ed.
- [28] M. Lieb and A. Meixner, *Opt. Express* **8**, 458 (2001).
- [29] R. K. Wangsness, *Electromagnetic fields* (Wiley, 1986), 2nd ed.
- [30] G. Leuchs, K. Mantel, A. Berger, H. Konermann, M. Sondermann, U. Peschel, N. Lindlein, and J. Schwider, *Applied Optics* **47**, 5570 (2008).
- [31] E. W. Streed, B. G. Norton, A. Jechow, T. J. Weinhold, and D. Kielpinski, *Phys. Rev. Lett.* **106**, 010502 (2011).
- [32] L. Mandel and E. Wolf, *Optical Coherence and Quantum Optics* (Cambridge University Press, Cambridge, New York, 1995), ISBN 0 521 41711 2.
- [33] E. Hecht, *Optics* (Addison-Wesley Publishing Company, 1987).
- [34] S. J. van Enk and H. J. Kimble, *Phys. Rev. A* **63**, 023809 (2001).
- [35] We note that recently the approach we follow here has been applied for the case of an aplanatic lens [21].